ACS Photonics

pubs.acs.org/journal/apchd5

Article

Ligand-Assisted Sulfide Surface Treatment of $CsPbI_3$ Perovskite Quantum Dots to Increase Photoluminescence and Recovery

Kim Anh Huynh,[#] Sa-Rang Bae,[#] Tuan Van Nguyen,[#] Ha Huu Do, Do Yeon Heo, Jinwoo Park, Tae-Woo Lee, Quyet Van Le,* Sang Hyun Ahn,* and Soo Young Kim*

Cite This: *ACS Photonics* 2021, 8, 1979−1987

Read Online

ACCESS | Metrics & More | Article Recommendations | Supporting Information

ABSTRACT: $CsPbI_3$ perovskite quantum dots (QDs) are more unstable over time as compared to other perovskite QDs, owing to ligand loss and phase transformation. The strong red emission from fresh $CsPbI_3$ QDs gradually declines to a weak emission from aged QDs, which PLQY dropped by 93% after a 20 day storage; finally, there is no emission from δ-phase $CsPbI_3$. The present study demonstrated a facile surface treatment method, where a sulfur−oleylamine (S-OLA) complex was utilized to passivate the defect-rich surface of the $CsPbI_3$ QDs and then self-assembly to form a matrix outside the $CsPbI_3$ QDs protected the QDs from environmental moisture and solar irradiation. The PLQY of the treated $CsPbI_3$ QDs increased to 82.4% compared to initial value of 52.3% of the fresh QDs. Furthermore, there was a significant increase in the colloidal stability of the $CsPbI_3$ QDs. Above 80% of the original PLQY of the treated QDs was reserved after a 20 day storage and the black phase could be maintained for three months before transforming to the yellow phase. The introduction of S-OLA induced the recovery of the lost photoluminescence of the nonluminous aged $CsPbI_3$ QDs with time to 95% of that of the fresh QDs. Furthermore, the photoluminescence was maintained for one month. The increase in the stability and photoluminescence are critical for realizing high-performance perovskite-QD-based devices. Therefore, this work paves the way for increasing the performance of perovskite-based devices in the near future.

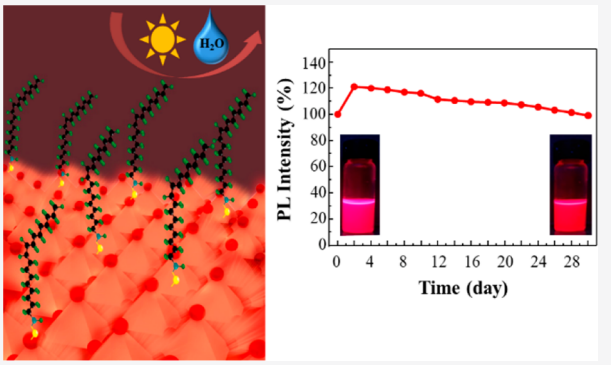

KEYWORDS: *lead-halide perovskite, $CsPbI_3$ quantum dots, surface treatment, photoluminescence intensity, stability*

Downloaded via SEOUL NATL UNIV on November 11, 2021 at 01:48:01 (UTC).
See https://pubs.acs.org/sharingguidelines for options on how to legitimately share published articles.

Lead halide perovskites ($APbX_3$; A = methylammonium (MA), formamidinium (FA), or cesium (Cs) and X = Cl^-, Br^-, or I^- or a combination thereof) are widely utilized in photovoltaic and optoelectronic applications owing to their outstanding optical and electrical properties. They are inexpensive substances with tunable bandgaps,[1] high light-absorption efficiencies, low exciton binding energies (e.g., 10 meV for $MAPbI_3$),[2] high photoluminescence quantum yields (PLQYs) of up to 100%,[3,4] and high charge-carrier mobilities of tens of $cm^2\ V^{-1}\ s^{-1}$.[5] These perovskites have been recently applied as efficient emissive layers in light-emitting diodes (LEDs),[6−8] light-absorbing layers in solar cells[9−13] and photodetectors,[14−16] and active films in gas sensors.[17,18] They have also been utilized in memory devices[19−21] and for photocatalysis.[22] The research on perovskite solar cells has advanced rapidly in the past decade. A substantial increase has been achieved in the power conversion efficiency from 3.8%, with an active area of 0.24 cm^2 (2009) to 23.7% with large-area devices (>1 cm^2) and modules (10 cm^2).[23] There has been marked growth in the external quantum emission of lead-halide perovskite LEDs to greater than 20% with multicolor from green to red.[24−26] The flexible perovskite LEDs were also first made in 2014.[27] The intensive research on electron and hole transport layers has also contributed to the increase in the power conversion efficiency of perovskite solar cells.[28,29]

Initially, organometallic halide perovskites were developed for photovoltaic applications (e.g., $MAPbI_3$ in 2009). However, all-inorganic halide perovskites have attracted significant research interest in recent times owing to their higher stabilities as compared to those of organometallic halide perovskites.[30] All-inorganic cesium halides ($CsPbX_3$) in the form of colloidal quantum dots (QDs) exhibit excellent PLQYs of greater than 90%.[31,32] Cesium lead iodide ($CsPbI_3$) is the most suitable candidate among the inorganic halide perovskites for application in photovoltaic devices owing to its optimal bandgap (~1.73 eV). The deep red emission (650−700 nm) from $CsPbI_3$ is also promising for display applications and solid-state lighting. The application of warm-white LEDs in lighting applications and red LED in horticultural lighting is

Received: December 24, 2020
Published: July 2, 2021

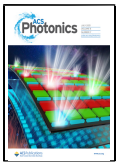

© 2021 American Chemical Society

https://doi.org/10.1021/acsphotonics.0c01952
ACS Photonics 2021, 8, 1979−1987

important and requires extensive studies. However, $CsPbI_3$ undergoes rapid phase transition,[33] which is attributed to the strong ionic bond of Cs^+ with the $[PbX_6^+]^{4-}$ octahedron. The Goldschmidt tolerance factor and the octahedral factor of $CsPbI_3$ are 0.893 and 0.47, respectively, and these values are borderline.[34] Marronnier et al. investigated the phase transition pathway of $CsPbI_3$.[35] The results revealed that cooling results in the transformation of the cubic α phase to the orthorhombic δ phase, while heating results in the reverse transformation to the α phase. Swarnkar et al. reported that nanoscale α-$CsPbI_3$ QDs, which are capped by organic ligands, are stable at low temperatures.[36] The use of nanosized organometal halide perovskites is beneficial for size adjustment. This not only ensures tunable bandgaps, but also facilitates surface treatment that increases the stability of the perovskite.[37] However, the capping ligands can easily desorb from the QD surface because of their dynamic nature and the ionic nature of QDs. Ligand loss generates directly exposed atoms and traps at the surface of QDs.[38,39] This induces a rapid decrease in the luminescent emission and the stability. The sensitivity of $CsPbI_3$ QDs to temperature, radiation, and humidity is higher than that of $CsPbBr_3$ QDs. The $CsPbI_3$ QDs that exhibit strong red emission gradually lose their luminescence within a short duration and do not emit any light under UV irradiation.[40] This is attributed to the ligand loss and the phase transformation. Various strategies, such as A-site doping, B-site doping, and ligand modulation, have been developed to stabilize the cubic α phase of $CsPbI_3$ QDs.[34] Wasim et al. successfully doped $CsPbI_3$ with 4.8% Mn via a postsynthesis method to achieve the long-term stability (one month) of the black perovskite phase.[41] The B-site exchange induces the blue-shift of the optical spectra due to the perovskite lattice contraction.[42] The surface treatment methods, which have limited impact on the perovskite structures, have been developed to passivate the surface and decrease the photoluminescence (PL) loss of $CsPbI_3$. There have been studies on the use of phosphine and phosphonic acid derivatives, including trioctylphosphine (TOP),[43] trioctylphosphine bis-(2,2,4-trimethylpentyl)phosphonic acid,[44] and a (TOP)−PbI_2 complex,[45] to passivate the surface of $CsPbI_3$ QDs; thus, the colloidal stability of $CsPbI_3$ QDs can be increased. The phosphine oxide molecule was utilized to passivate the QD film, which produced high efficiency perovskite QD-based LEDs.[46] The application of 2,2-iminodibenzoic acid or μ-graphene to stabilize the cubic phase of $CsPbI_3$ has also been explored. However, these organic compounds are hazardous. Therefore, a facile surface treatment using sodium sulfide, which is more ecofriendly than phosphine-based compounds, was developed in the present study to increase the PL intensity and colloidal stability of $CsPbI_3$ QDs. The treatment involved the combination of S^{2-}, which was dissociated from Na_2S, with oleylamine (OLA) in hexane or toluene (marked as S-OLA). The $CsPbI_3$ QDs were synthesized using the hot-injection method and treated with different amounts of S-OLA. S-OLA acted as an etchant and removed the nonradiative defects on the surfaces of the $CsPbI_3$ QDs. Furthermore, it passivated the surfaces of the $CsPbI_3$ QDs, thereby ensuring protection from humidity and solar irradiation. When the nonemissive aged $CsPbI_3$ QDs were treated with S-OLA, their PL emission was gradually recovered and maintained for a month.

EXPERIMENTAL SECTION

Chemicals. Cesium carbonate (Cs_2CO_3, 99.9% (with trace metals)), lead(II) iodide (PbI_2, 99.999%), oleic acid (OA, technical grade, 90%), OLA (technical grade, 70%), 1-octadecene (ODE, technical grade, 90%), butylamine (BTA, 99.5%), octylamine (OTA, 99%), dodecylamine (DDA, 98%), and sodium sulfide (Na_2S) were purchased from MilliporeSigma, Missouri, U.S.A. Methyl acetate (MeOAc, anhydrous, 99%) was purchased from Alfa Aesar (Thermo Fisher Scientific), Massachusetts, U.S.A. All the chemicals were used as purchased without further purification.

Synthesis and Purification of the $CsPbI_3$ QDs. Initially, 326 mg of Cs_2CO_3 was loaded into a 100 mL three-neck flask with 16 mL of ODE and 1 mL of OA. The solution was dried for 1 h at 120 °C and then heated to 150 °C until the complete reaction of the entire Cs_2CO_3 with OA. This solution was kept in stock and preheated before use.

Subsequently, 30 mL of ODE, 520 mg of PbI_2, 3 mL of OA, and 3 mL of OLA were loaded into a 100 mL three-neck flask. The flask was filled with N_2, and the contents were stirred under a constant N_2 flow at 120 °C. The temperature of the solution was increased to 160 °C after the complete dissolution of PbI_2. Thereafter, 2.4 mL of the prepared preheated Cs-oleate solution was rapidly injected into the solution, and the reaction mixture was cooled in an ice bath after a 5 s reaction. MeOAc (60 mL) was added to the reaction mixture, which was then centrifuged at 8000 rpm for 10 min. Subsequently, the precipitate was dispersed in 120 mL of hexane and centrifuged again to remove the unreacted PbI_2 and the aggregates. The as-synthesized $CsPbI_3$ QD solution was marked as a fresh sample. The fresh sample that was stored under ambient conditions for 20 days was marked as the aged sample.

Surface Treatment. The surface treatment involved the dissolution of 39 mg of Na_2S into 10 mL of hexane and 100 μL of OLA in a 20 mL vial. This solution was stirred overnight. The use of short-chain amines to assist the loading of S^{2-} on the surfaces of the QDs was also examined. Decantation was performed to obtain 0.05 M S-OLA (C18), S-DDA (C12), and S-OTA (C8) in the hexane solution. The S-amine solution (20, 40, 60, 80, and 100 μL) was added to 2 mL of the as-synthesized $CsPbI_3$ QDs. The mixture was kept undisturbed for 1 day and centrifuged to obtain the final products, that is, the fresh-treated-20, fresh-treated-40, fresh-treated-60, fresh-treated-80, and fresh-treated-100 samples. The surface treatment reactions were conducted on both the fresh and aged samples.

Characterization. The ultraviolet−visible (UV−vis) absorption spectra were obtained using UV−vis spectrophotometry (Varian Inc. (Agilent Technologies, Inc.), California, U.S.A.). The fluorescence spectra were obtained via fluorescence spectrophotometry (Varian Inc. (Agilent Technologies, Inc.), California, U.S.A.). The structure of the resulting QDs was analyzed via X-ray diffraction (XRD) and transmission electron microscopy (TEM). The presence of S was determined using X-ray photoelectron spectroscopy (XPS) and energy-dispersive X-ray spectroscopy (EDS). PL lifetime was measured by FluoTime 300. Picosecond-pulse laser head (LDH-P-C-405B, PicoQuant) was used to excite the samples with a laser of 405 nm wavelength. Photon counting detector (PMA Hybrid 07) and time-correlated single photon counting (TCSPC) module (PicoHarp, PicoQuant) were used to detect the PL decay and calculate the PL lifetime of samples. PLQY of

https://doi.org/10.1021/acsphotonics.0c01952
ACS Photonics 2021, 8, 1979−1987

perovskite QDs solutions was measured using a JASCO FP8500 spectrofluorometer that was equipped with a 100 mm integrating sphere (ILF-835). The PLQY values were calculated by Jasco SpectraManager II software.

RESULTS AND DISCUSSION

The experiment was performed under ambient conditions (30 °C and 80% relative humidity), and all the samples were stored under the ambient conditions without inert gas protection. The $CsPbI_3$ QDs were synthesized using the hot-injection method. Subsequently, they were washed with methyl acetate, separated from the crude solution via centrifugation, and dispersed in hexane to form the fresh $CsPbI_3$ QDs. During stirring Na_2S in hexane along with oleylamine, the oleylamine was transferred to the oleylammonium form ($C_{18}H_{35}NH_3^+$), then interacted with S^{2-} as an ion pair ($C_{18}H_{35}NH_3^+-S^{2-}$). Different quantities of the S-OLA solution (20, 40, 60, 80, and 100 μL) were added to 2 mL each of the fresh QDs. The passivation treatment of the surfaces of the QDs happened, as illustrated in Scheme 1. When S-OLA was introduced to the QD solution, it was adsorbed on the surface of the QDs, inducing an initial decrease in PL; however, the peak position was still maintained at 693 nm. Under the etching effect of S-OLA, the surface cesium cations Cs^+ and iodide anions I^- were likely to dissolve into solution. Meanwhile, a quantity of S-OLA was strongly anchored on the surface via the interatomic interaction of S and exposed Pb to form Pb−S bonds.[47] Therefore, a blue-shift was witnessed and the PL was recovered after the completion of the passivation (Figure S1). This new ligand layer helped to remove surface trap defects and protected the $CsPbI_3$ QDs from impact of humidity because of the lower solubility of PbS compared to PbI_2.

Scheme 1. Schematic Illustration of the Mechanism of the Passivation Treatment with S-OLA on the $CsPbI_3$ QD Surfaces

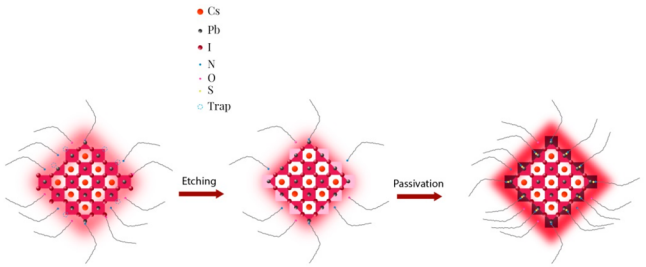

Figure 1 presents the evolution in the optical properties of the $CsPbI_3$ QDs after the treatment. The absorption curves of the fresh-treated samples were identical to those of the fresh samples (Figure 1a). The intensity of the PL of the treated samples gradually increased then decreased as the volume of S-OLA increased from 0 to 100 μL with the maximum value was reached at 60 μL (Figure 1b). Consistently, the PLQY witnessed an increase from 52.3% in initial to 82.4% (Figure 1d) with the addition of 60 μL of S-OLA then decreased to 79% and 74.9% when the volume of S-OLA surpassed 60 μL. This indicated that the presence of excess S^{2-} lowered the PL emission from the QDs. The increase in the PL intensity with the increase in the volume of S-OLA accompanied the blue-shift of the PL peak that was attributed to the passivation effect (Figure 1c). The passivation of trap states can blue-shift the PL peak because the spontaneous radiative recombination between them can red-shift the emission peak compared with that from the band edge transition.[48]

Short-chain amines (C12 and C8) were also utilized as ligands to assist the loading of S^{2-} on the surfaces of the QDs. The effects of the addition of DDA (C12) and octylamine (C8) were similar to those of the addition of OLA (C18)

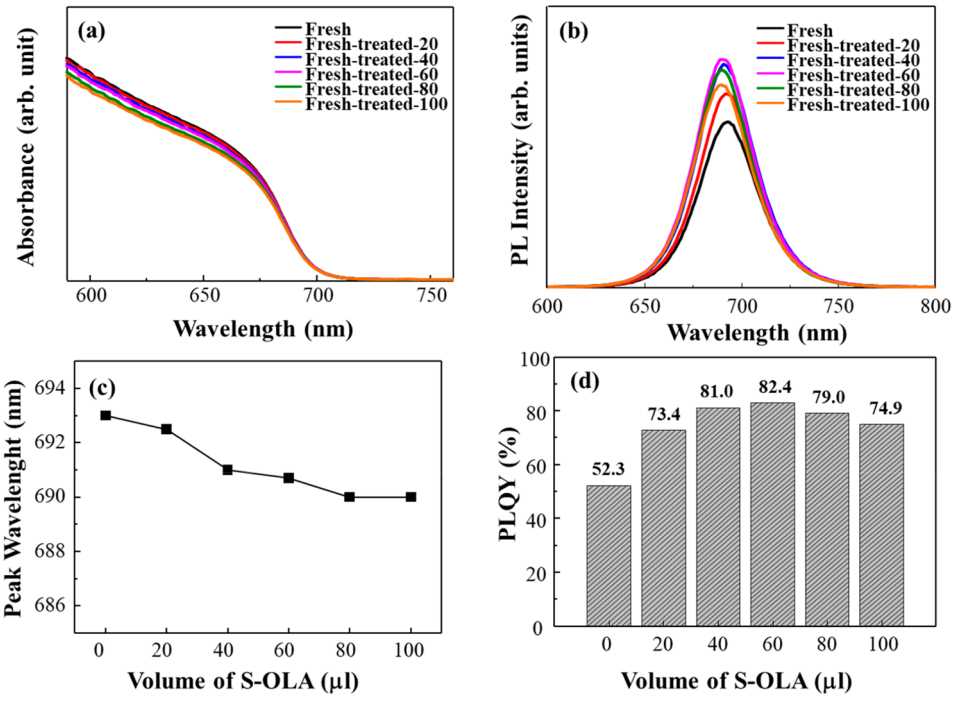

Figure 1. (a) Absorption spectra, (b) PL spectra, (c) PL wavelength peaks, and (d) PLQY of the fresh $CsPbI_3$ QDs treated with different amounts of S-OLA after 1 day.

https://doi.org/10.1021/acsphotonics.0c01952
ACS Photonics 2021, 8, 1979−1987

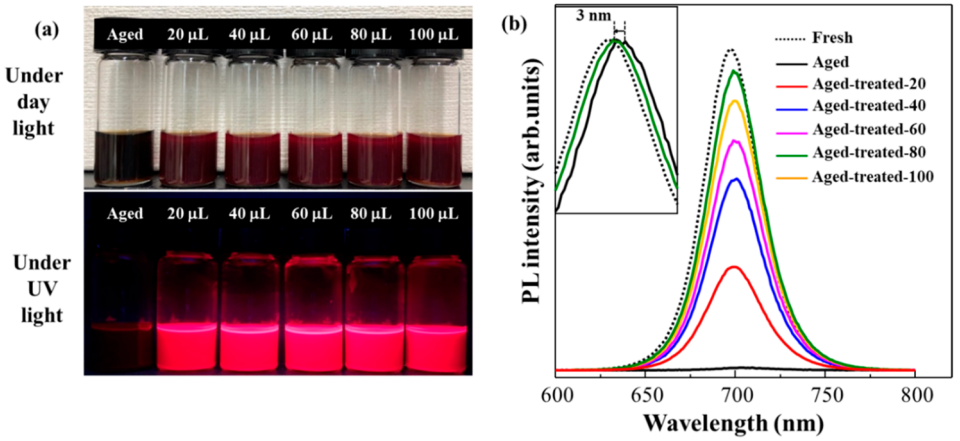

Figure 2. (a) Photos of the aged $CsPbI_3$ QDs with different amounts of S-OLA under daylight (top) and UV light (wavelength = 365 nm; bottom). (b) PL spectra of the aged $CsPbI_3$ QDs with different amount of S-OLA.

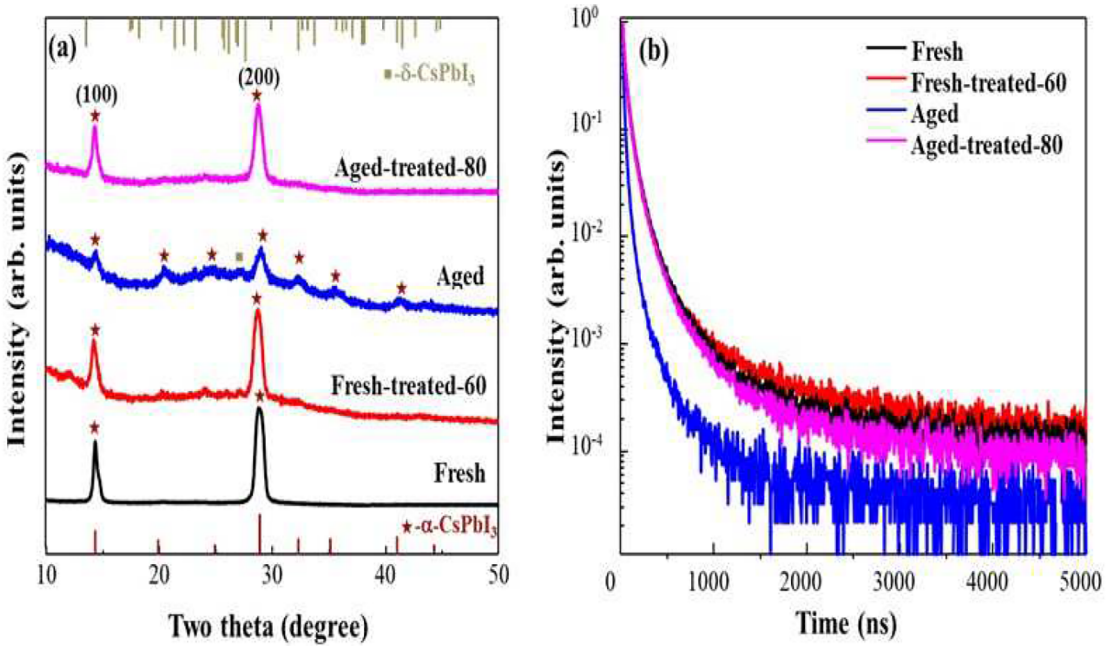

Figure 3. (a) XRD patterns and (b) time-resolved PL spectra of the fresh, fresh-treated (60 μL of S-OLA), aged, and aged-treated (80 μL S-OLA) $CsPbI_3$ QDs.

(Figure S2). This observation confirmed that the passivation ability of S^{2-} on the surfaces of the QDs decreased the surface defects; thus, the nonradiative recombination was also decreased. Therefore, there was an increase in the PL intensity of the fresh-treated QDs. According to the absorption spectra of the aged and aged-treated $CsPbI_3$ QDs shown in Figure S3, S-OLA treatment did not affect the bandgap of aged samples. Furthermore, the PL spectra of OLA and S-OLA samples shown in Figure S4 indicated that S-OLA treatment is more effective than OLA treatment.

The fresh $CsPbI_3$ QD solution gradually turned dark after prolonged storage. The fluorescence emission was steadily quenched over 20 days (aged QDs); subsequently, it underwent decay. The PLQY of the aged QD solutions, indicated by the black solid line in Figure 2b, dropped to 3.5%, indicated by the black dotted line in Figure 2b. The fluorescence of the aged $CsPbI_3$ QD solutions was recovered after the introduction of S-OLA. The aged QD solutions transformed from black to bright red and exhibited strong red emission under UV light (Figure 2a) after the addition of S-OLA. The PL intensity of the aged QDs was recovered to 59% of the initial intensity of the fresh $CsPbI_3$ QDs after the addition of 20 μL of S-OLA. The PL intensity of the aged QDs continued to increase with the increase in the volume of S-OLA and reached 95% of the initial intensity of the fresh QDs with the addition of 80 μL of S-OLA. The PL peaks of the aged QDs were red-shifted by 4 nm as compared to those of the fresh QDs. However, the PL peak of the sample that was treated with 80 μL of S-OLA exhibited a blue-shift of approximately 3 nm (inset of Figure 2b) after the treatment, which was consistent with the previous reports.[49]

Figure 3a shows the evolution of the XRD patterns of both the fresh and aged $CsPbI_3$ QDs before and after the treatment. The two primary peaks at 14.3° and 28.8° in the XRD patterns corresponded to the (100) and (200) planes of bulk perovskites. The XRD patterns for the fresh and fresh-treated

https://doi.org/10.1021/acsphotonics.0c01952
ACS Photonics 2021, 8, 1979−1987

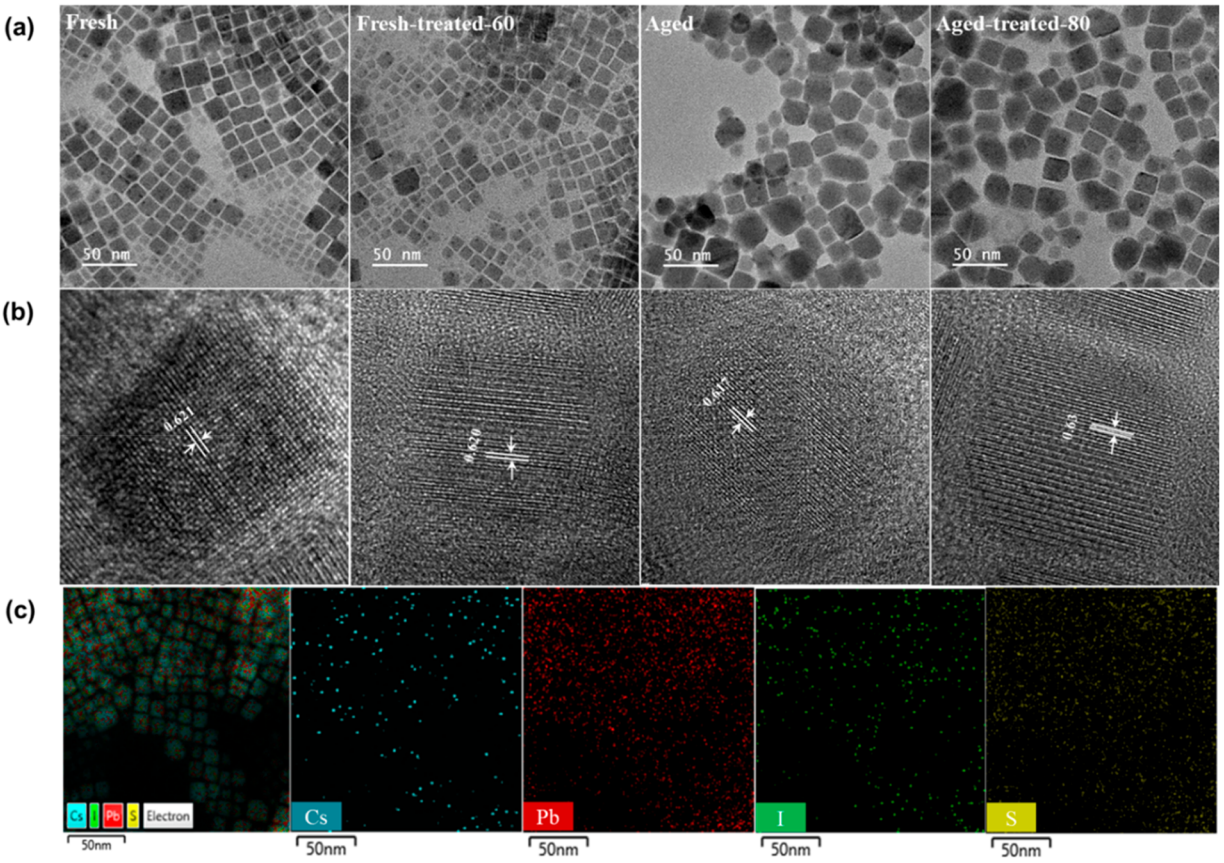

Figure 4. (a) TEM images (50 nm scale bar) and (b) HRTEM images (5 nm scale bar) of the fresh, fresh-treated, aged, aged-treated $CsPbI_3$ QDs. (c) EDS mapping of the fresh-treated $CsPbI_3$ QDs.

samples were similar. This indicated that S^{2-} did not exert any significant effect on the crystal structure of the $CsPbI_3$ QDs. The magnification of the peaks at 14.3° and 28.8° in the XRD patterns of the fresh-treated samples revealed a slight peak shift toward lower angles. This might be attributed to the compressive internal stresses or the lattice dilation.[50] The XRD spectra in Figure S5 showed that all the fresh-treated samples remained in the cubic α phase. Distinct PbS peaks were observed in the XRD patterns of the fresh-treated-80 and fresh-treated-100 QDs. This might have resulted in the decrease in the PL intensity with the increase in the volume of S-OLA beyond 60 μL. Prolonged aging resulted in the appearance of new peaks in the XRD patterns of the aged QDs. Furthermore, the two primary peaks at 14.3° and 28.8° in the XRD patterns shifted toward higher angles. This indicated the occurrence of phase transformation. The new peaks disappeared after the addition of S-OLA, while the intensities of the two primary peaks increased.

The time-resolved PL decay curves were fitted by triexponential decay functions of $I(t) = A_1e^{-t/\tau_1} + A_2e^{-t/\tau_2} + A_3e^{-t}/^{\tau_3}$. The average PL lifetime was calculated by $\tau_{avg} = (A_1\tau_1^2 + A_2\tau_2^2 + A_3\tau_3^2)/(A_1\tau_1 + A_2\tau_2 + A_3\tau_3)$. The time-resolved PL increased from 61.6 ns for the fresh $CsPbI_3$ QDs to 68.1 ns for fresh-treated-60 QDs due to the suppression of nonradiative surface defects (Figure 3b and Table S1). This result further confirmed the passivation effect of S-OLA on the surface of $CsPbI_3$ QDs. Furthermore, the PL lifetime of aged QDs also showed an increase after treatment, from 5.1 ns to 53.5 ns. This is because of the suppression of abundant nonradiative combination centers formed during aging.

The Fourier transform infrared (FTIR) spectrum of four kinds of samples are exhibited in Figure S6. The OLA and OA exist as oleate and oleylammonium for perovskite QD ligands that is presented by signals at 1646 and 1638 cm^{-1}, respectively.[51,52] These signals were exhibited on fresh QDs. After aging, the peak of COO^- and NH_3^+ is reduced and a new peak at 1710 cm^{-1} that corresponded to C═O stretching of −COOH. This means during storage, the removal of ligands occurred along with the transformation from oleate species to OA that weakens the ligand shell protection. The C═O stretching of OA confirmed the occurrence of ligand exchange. The absence of the C═O stretching and the presence of the strong N−H peak in the FTIR spectra of the aged treated samples suggested that OA was replaced by the S-OLA complex after the treatment. Bodnarchuk et al. reported that the presence of excess OA accelerated the decrease in the fluorescence quantum yield during storage. Therefore, the replacement of the undesirable oleate group with S-OLA facilitated the increase in the stability of the QDs. On the other hand, we can see that the intensity of strong sharp C−H stretching of the long alkyl chain of ligand at 2800−3000 cm^{-1} in the aged QDs reduced compared to that of the fresh QDs. This is because of the removal of ligands during storage. These peaks become stronger after passivation that confirms binding of more ligands to the QD surface.

The TEM images of the fresh and fresh-treated QDs indicated the presence of cubic particles with average sizes of 15.2 and 14.3 nm, respectively (Figure 4a), which was in line with the blue-shift in PL results.[53] A well-defined cubic structure with a lattice spacing of 0.62 nm was observed in the

https://doi.org/10.1021/acsphotonics.0c01952
ACS Photonics 2021, 8, 1979−1987

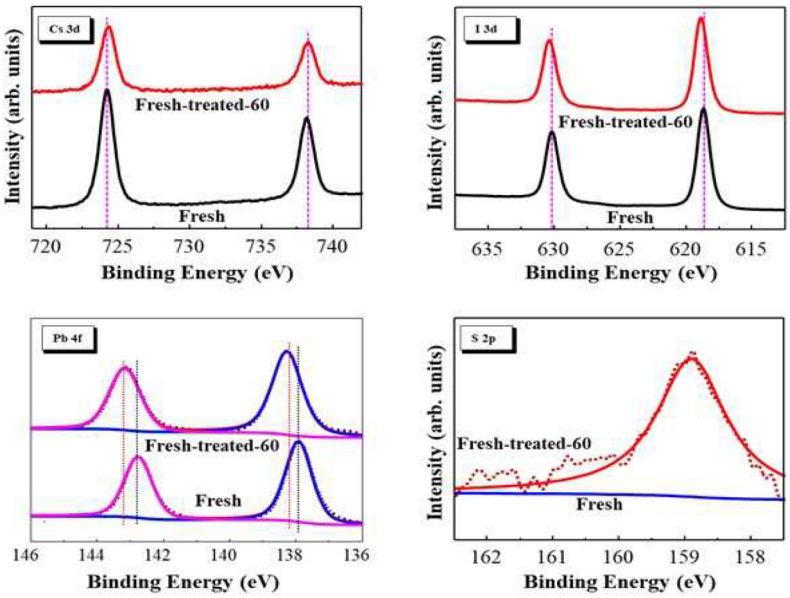

Figure 5. High-resolution XPS spectra of Cs 3d, I 3d, Pb 4f, and S 2f of the fresh and fresh-treated $CsPbI_3$ QDs.

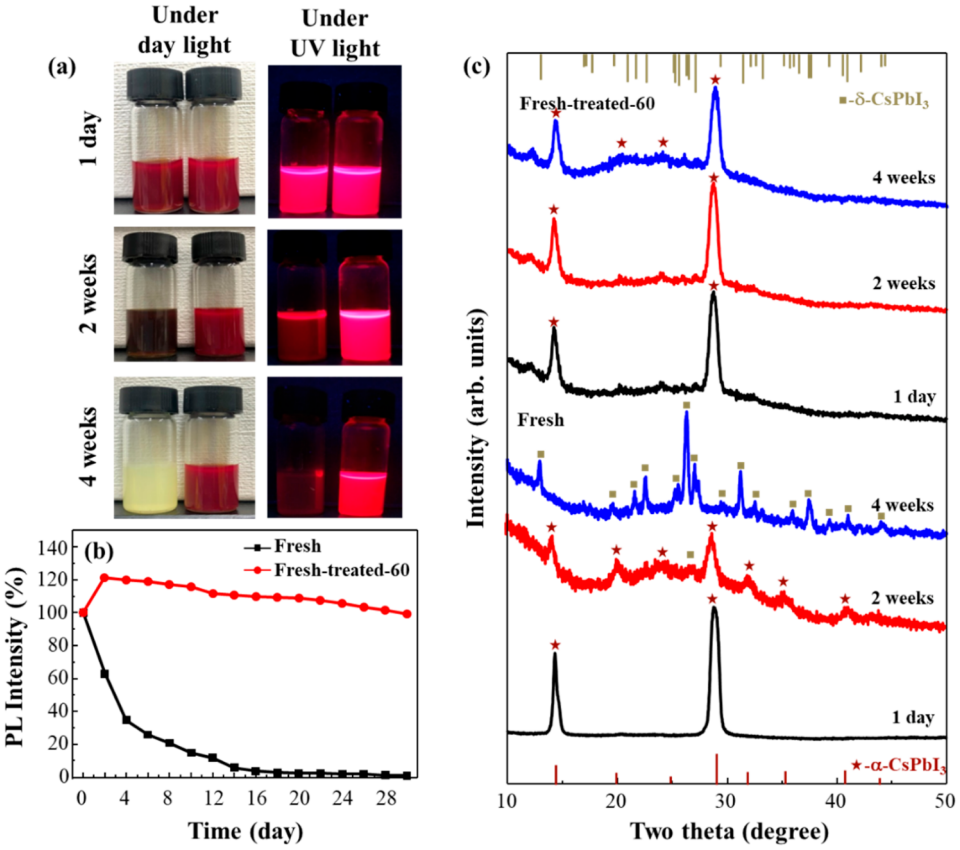

Figure 6. (a) Colloidal solutions of the fresh and fresh-treated-60 QDs under daylight and UV light. (b) Stability of the PL intensity over time. (c) Normalized XRD patterns after the storage of the fresh and fresh-treated-60 QDs for different times.

high-resolution (HR) TEM images of both the fresh and fresh-treated QDs (Figure 4b). The sizes of the QDs slightly decreased after the passivation treatment, thereby confirming the removal of nonradiative defects from the surface. These results were consistent with the increase in the full width at half-maximum (fwhm) of the XRD peaks from 0.81 to 0.85.

The aged QDs became larger after prolonged storage, and their corners became rounded. This was attributed to the loss of the ligands from the surface of the QDs that resulted in aggregation and phase transformation. The sizes of the aged and regenerated QDs were 21.6 nm (lattice spacing = 0.617 nm) and 20.4 nm (lattice spacing = 0.63 nm), respectively. Marronnier et al. reported that when the α phase with the

https://doi.org/10.1021/acsphotonics.0c01952
ACS Photonics 2021, 8, 1979−1987

$Pm\bar{3}m$ space group transformed to the γ phase with the *Pbnm* space group, the decrease in the lattice constants corresponded to the decrease in the lattice spacing.[35] This indicated the occurrence of phase transformation during aging. The decrease in the size of the QDs after the treatment with S-OLA corresponded to the blue-shift in the PL position. This observation was consistent with that in a previous report, where the size of the perovskite decreased under vigorous stirring in the presence of ligands.[47,54,55] The spacing between the QDs not only became more uniform but also increased after the treatment with S−OLA. This indicated the absorption of new ligands on the surfaces of the QDs. The results of the EDS mapping of the fresh-treated $CsPbI_3$ QDs (Figure 4c) elucidated the interaction between S-OLA and the surfaces of the QDs. S^{2-} was evenly distributed with Pb in the $CsPbI_3$ crystals. This indicated that the strong affinity between S-OLA and Pb resulted in the binding of S-OLA with Pb on the surfaces of the QDs. Size distribution histograms of fresh, fresh-treated-60, aged, aged-treated-80 $CsPbI_3$ QDs are shown in Figure S6.

XPS analysis was conducted using the fresh and fresh-treated QDs to elucidate the bond and valence states of the elements in the $CsPbI_3$ QDs before and after passivation. Figure 5 shows the high-resolution XPS spectra of Cs 3d, I 3d, Pb 4f, and S 2p that were calibrated with C 1s. The Pb 4f and I 3d peaks shifted to higher binding energies in the XPS spectra of the fresh-treated $CsPbI_3$ QDs as compared to those in the XPS spectra of the fresh QDs after the incorporation of S^{2-}. However, no peak shift was observed for Cs 3d. The peaks in the Pb 4f spectrum that corresponded to the $4f_{7/2}$ and $4f_{5/2}$ oxidation states of Pb shifted from 137.9 to 138.3 eV and 142.8 to 143.1 eV, respectively. This shift could be caused by the formation of stronger ionic bonding between Pb^{2+} and S^{2-}.[56] The peaks in the I 3d spectrum that corresponded to the $3d_{5/2}$ and $3d_{3/2}$ oxidation states of I shifted from 618.7 to 618.9 eV and 630 to 630.3 eV, respectively. These shifts were ascribed to the adjustment in the chemical bonding between Pb^{2+} and I^- owing to the incorporation of S^{2-}. The presence of the S 2p peak at 158.8 eV was detected in the treated sample. This suggested the formation of the S−Pb bond that was consistent with the results of EDS mapping.[57]

The fresh and fresh-treated $CsPbI_3$ QD solution was stored in air, and the variation in the relative PL intensity with time was recorded. Thus, the stability of the colloidal $CsPbI_3$ QDs was determined. The PL intensity of the fresh QD solution decreased by 30% after 1 day; subsequently, it decreased to 20% and 5% of the initial intensity after 7 and 15 days, respectively (Figure 6b). New defects were formed owing to the loss of the OLA and OA ligands from the surfaces of the QDs. The PL intensity of the treated $CsPbI_3$ QDs decreased to 92% of the intensity of the fresh QDs after 7 days, before leveling off at approximately 80% of the initial intensity. A total of 30 days of storage under the ambient conditions induced the transformation of the fresh $CsPbI_3$ QDs to the yellow δ phase; however, the fresh-treated QDs remained in the black phase (Figure 6a) with only a 20% decrease in their PL intensity (Figure 6c). The black phase of fresh-treated QDs was stable for more than three months before transforming to yellow nonperovskite phase. These results indicated that the S-OLA complex was effectively absorbed on the surfaces of the QDs, unlike that for OLA/OA, owing to the strong affinity between S and Pb. This suppressed not only the ligand loss from the surfaces of the QDs but also the formation of new defects. Moreover, this passivation could protect the surface of QDs from humidity because of extremely low solubility of PbS compared to PbI_2.[56] Thus, the PL loss was successfully inhibited. Furthermore, with passivation, the lifetime reduced from 68.1 to 51.3 ns after aging while a remarkable decrease from 61.6 to 5.1 ns was observed in fresh QDs (Table S1). Without passivation, the native ligand easily desorb from the surface leaving the surface trap states as nonradiative defects resulting in degradation of the optical properties of colloidal. And without the protection of the ligand shell, the moisture easily comes in contact with QDs, causing phase transition.

CONCLUSIONS

The significant impact of the ligands and the surface defects on the PL emission from $CsPbI_3$ QDs was investigated in the present study. A facile surface passivation treatment using S-OLA was conducted to eliminate the surface defects of the $CsPbI_3$ QDs, thereby increasing the PLQY of the QDs from 52.3% to 82.4%. The treatment was effective for both the fresh and aged samples, and it increased the PL emission lifetime without disrupting the crystal structure. The suppression of the luminescence quenching over time in a highly humid environment indicated the adequate passivation of the surfaces of the QDs. The S-OLA ligands were effectively anchored to the $CsPbI_3$ QDs via Pb−S bonds after the passivation. Therefore, the ligand loss and the agglomeration of the QDs were prevented; the $CsPbI_3$ QD solution can retain its fluorescent phase for more than three months.

ASSOCIATED CONTENT

Supporting Information

The Supporting Information is available free of charge at https://pubs.acs.org/doi/10.1021/acsphotonics.0c01952.

Figures showing the evolution in the PL intensity of the $CsPbI_3$ QDs following the treatment with 60 μL of S-OLA, the PL intensities of the fresh perovskite QDs with different amine-assisted S^{2-} treatments, the absorption spectra of the aged and aged-treated $CsPbI_3$ QDs, and the XRD patterns of the fresh $CsPbI_3$ QDs with different amounts of S-OLA (PDF)

AUTHOR INFORMATION

Corresponding Authors

Quyet Van Le − *Institute of Research and Development, Duy Tan University, Da Nang 550000, Vietnam;* orcid.org/0000-0002-4313-301X; Email: levanquyet@dtu.edu.vn

Sang Hyun Ahn − *School of Chemical Engineering and Materials Science, Chung-Ang University, Seoul 06974, Republic of Korea;* orcid.org/0000-0001-8906-5908; Email: shahn@cau.ac.kr

Soo Young Kim − *Department of Materials Science and Engineering, Institute of Green Manufacturing Technology, Korea University, Seongbuk-gu, Seoul 02841, Republic of Korea;* orcid.org/0000-0002-0685-7991; Email: sooyoungkim@korea.ac.kr

Authors

Kim Anh Huynh − *School of Chemical Engineering and Materials Science, Chung-Ang University, Seoul 06974, Republic of Korea*

Sa-Rang Bae − *Department of Materials Science and Engineering, Institute of Green Manufacturing Technology,*

https://doi.org/10.1021/acsphotonics.0c01952
ACS Photonics 2021, 8, 1979−1987

Korea University, Seongbuk-gu, Seoul 02841, Republic of Korea

Tuan Van Nguyen − *School of Chemical Engineering and Materials Science, Chung-Ang University, Seoul 06974, Republic of Korea*

Ha Huu Do − *School of Chemical Engineering and Materials Science, Chung-Ang University, Seoul 06974, Republic of Korea*

Do Yeon Heo − *Department of Materials Science and Engineering, Institute of Green Manufacturing Technology, Korea University, Seongbuk-gu, Seoul 02841, Republic of Korea*

Jinwoo Park − *Department of Materials Science and Engineering, Seoul National University, Gwanak-gu, Seoul 08826, Republic of Korea*

Tae-Woo Lee − *Department of Materials Science and Engineering, School of Chemical and Biological Engineering, Institute of Engineering Research, Research Institute of Advanced Materials, Nano Systems Institute (NSI), Seoul National University, Gwanak-gu, Seoul 08826, Republic of Korea;* orcid.org/0000-0002-6449-6725

Complete contact information is available at: https://pubs.acs.org/10.1021/acsphotonics.0c01952

Author Contributions

#K.A.H., S.-R.B., and T.V.N. contributed equally to this work.

Notes

The authors declare no competing financial interest.

■ ACKNOWLEDGMENTS

This research was supported by the National Research Foundation of Korea (NRF; NRF-2020R1A2C2100670).

■ REFERENCES

(1) Protesescu, L.; Yakunin, S.; Bodnarchuk, M. I.; Krieg, F.; Caputo, R.; Hendon, C. H.; Yang, R. X.; Walsh, A.; Kovalenko, M. V. Nanocrystals of Cesium Lead Halide Perovskites ($CsPbX_3$ X = Cl, Br, and I) Novel Optoelectronic Materials Showing Bright Emission with Wide Color Gamut. *Nano Lett.* **2015**, *15* (6), 3692−3696.

(2) Chen, X.; Lu, H.; Yang, Y.; Beard, M. C. Excitonic Effects in Methylammonium Lead Halide Perovskites. *J. Phys. Chem. Lett.* **2018**, *9* (10), 2595−2603.

(3) Liu, F.; Zhang, Y.; Ding, C.; Kobayashi, S.; Izuishi, T.; Nakazawa, N.; Toyoda, T.; Ohta, T.; Hayase, S.; Minemoto, T.; Yoshino, K.; Dai, S.; Shen, Q. Highly Luminescent Phase-Stable $CsPbI_3$ Perovskite Quantum Dots Achieving Near 100% Absolute Photoluminescence Quantum Yield. *ACS Nano* **2017**, *11* (10), 10373−10383.

(4) Di Stasio, F.; Christodoulou, S.; Huo, N.; Konstantatos, G. Near-Unity Photoluminescence Quantum Yield in $CsPbBr_3$ Nanocrystal Solid-State Films via Postsynthesis Treatment with Lead Bromide. *Chem. Mater.* **2017**, *29* (18), 7663−7667.

(5) Herz, L. M. Charge-Carrier Mobilities in Metal Halide Perovskites: Fundamental Mechanisms and Limits. *ACS Energy Lett.* **2017**, *2* (7), 1539−1548.

(6) Le, Q. V.; Kim, J. B.; Kim, S. Y.; Lee, B.; Lee, D. R. Structural Investigation of Cesium Lead Halide Perovskites for High-Efficiency Quantum Dot Light-Emitting Diodes. *J. Phys. Chem. Lett.* **2017**, *8* (17), 4140−4147.

(7) Li, Y.-F.; Feng, J.; Sun, H.-B. Perovskite Quantum Dots for Light-Emitting Devices. *Nanoscale* **2019**, *11* (41), 19119−19139.

(8) Van Le, Q.; Park, M.; Sohn, W.; Jang, H. W.; Kim, S. Y. Investigation of Energy Levels and Crystal Structures of Cesium Lead Halides and Their Application in Full-Color Light-Emitting Diodes. *Adv. Electron. Mater.* **2017**, *3* (1), 1600448.

(9) Zhao, Q.; Hazarika, A.; Chen, X.; Harvey, S. P.; Larson, B. W.; Teeter, G. R.; Liu, J.; Song, T.; Xiao, C.; Shaw, L.; Zhang, M.; Li, G.; Beard, M. C.; Luther, J. M. High Efficiency Perovskite Quantum Dot Solar Cells with Charge Separating Heterostructure. *Nat. Commun.* **2019**, *10* (1), 2842.

(10) Li, F.; Zhou, S.; Yuan, J.; Qin, C.; Yang, Y.; Shi, J.; Ling, X.; Li, Y.; Ma, W. Perovskite Quantum Dot Solar Cells with 15.6% Efficiency and Improved Stability Enabled by an α-$CsPbI_3$/$FAPbI_3$ Bilayer Structure. *ACS Energy Lett.* **2019**, *4* (11), 2571−2578.

(11) Ji, K.; Yuan, J.; Li, F.; Shi, Y.; Ling, X.; Zhang, X.; Zhang, Y.; Lu, H.; Yuan, J.; Ma, W. High-Efficiency Perovskite Quantum Dot Solar Cells Benefiting from a Conjugated Polymer-Quantum Dot Bulk Heterojunction Connecting Layer. *J. Mater. Chem. A* **2020**, *8* (16), 8104−8112.

(12) Karani, A.; Yang, L.; Bai, S.; Futscher, M. H.; Snaith, H. J.; Ehrler, B.; Greenham, N. C.; Di, D. Perovskite/Colloidal Quantum Dot Tandem Solar Cells: Theoretical Modeling and Monolithic Structure. *ACS Energy Lett.* **2018**, *3* (4), 869−874.

(13) Lee, H.; Kim, K.; Song, O. Properties of Perovskite Solar Cells with GO Addition on TiO_2 Layer. *Taehan Kumsok·Chaeryo Hakhoechi* **2019**, *57* (7), 456−461.

(14) Kwon, K. C.; Hong, K.; Van Le, Q.; Lee, S. Y.; Choi, J.; Kim, K. B.; Kim, S. Y.; Jang, H. W. Inhibition of Ion Migration for Reliable Operation of Organolead Halide Perovskite-Based Metal/Semiconductor/Metal Broadband Photodetectors. *Adv. Funct. Mater.* **2016**, *26* (23), 4213−4222.

(15) Bi, C.; Kershaw, S. V.; Rogach, A. L.; Tian, J. Improved Stability and Photodetector Performance of $CsPbI_3$ Perovskite Quantum Dots by Ligand Exchange with Aminoethanethiol. *Adv. Funct. Mater.* **2019**, *29* (29), 1902446.

(16) Dai, Z.; Ou, Q.; Wang, C.; Si, G.; Shabbir, B.; Zheng, C.; Wang, Z.; Zhang, Y.; Huang, Y.; Dong, Y.; Jasieniak, J. J.; Su, B.; Bao, Q. Capillary-Bridge Mediated Assembly of Aligned Perovskite Quantum Dots for High-Performance Photodetectors. *J. Mater. Chem. C* **2019**, *7* (20), 5954−5961.

(17) Kakavelakis, G.; Gagaoudakis, E.; Petridis, K.; Petromichelaki, V.; Binas, V.; Kiriakidis, G.; Kymakis, E. Solution Processed $CH_3NH_3PbI_{3-x}Cl_x$ Perovskite Based Self-Powered Ozone Sensing Element Operated at Room Temperature. *ACS Sens.* **2018**, *3* (1), 135−142.

(18) Zhu, Z.; Sun, Q.; Zhang, Z.; Dai, J.; Xing, G.; Li, S.; Huang, X.; Huang, W. Metal Halide Perovskites: Stability and Sensing-Ability. *J. Mater. Chem. C* **2018**, *6* (38), 10121−10137.

(19) Han, J. S.; Le, Q. V.; Choi, J.; Hong, K.; Moon, C. W.; Kim, T. L.; Kim, H.; Kim, S. Y.; Jang, H. W. Air-Stable Cesium Lead Iodide Perovskite for Ultra-Low Operating Voltage Resistive Switching. *Adv. Funct. Mater.* **2018**, *28* (5), 1705783.

(20) Choi, J.; Le, Q. V.; Hong, K.; Moon, C. W.; Han, J. S.; Kwon, K. C.; Cha, P.-R.; Kwon, Y.; Kim, S. Y.; Jang, H. W. Enhanced Endurance Organolead Halide Perovskite Resistive Switching Memories Operable under an Extremely Low Bending Radius. *ACS Appl. Mater. Interfaces* **2017**, *9* (36), 30764−30771.

(21) Li, B.; Hui, W.; Ran, X.; Xia, Y.; Xia, F.; Chao, L.; Chen, Y.; Huang, W. Metal Halide Perovskites for Resistive Switching Memory Devices and Artificial Synapses. *J. Mater. Chem. C* **2019**, *7* (25), 7476−7493.

(22) Huynh, K. A.; Nguyen, D. L. T.; Nguyen, V. H.; Vo, D. V. N.; Trinh, Q. T.; Nguyen, T. P.; Kim, S. Y.; Le, Q. V. Halide perovskite photocatalysis: progress and perspectives. *J. Chem. Technol. Biotechnol.* **2020**, *95* (10), 2579−2596.

(23) A Decade of Perovskite Photovoltaics. *Nat. Energy* **2019**, *4* (1), 1−1.

(24) Lin, K.; Xing, J.; Quan, L. N.; de Arquer, F. P. G.; Gong, X.; Lu, J.; Xie, L.; Zhao, W.; Zhang, D.; Yan, C.; Li, W.; Liu, X.; Lu, Y.; Kirman, J.; Sargent, E. H.; Xiong, Q.; Wei, Z. Perovskite Light-Emitting Diodes with External Quantum Efficiency Exceeding 20%. *Nature* **2018**, *562* (7726), 245−248.

(25) Chiba, T.; Hayashi, Y.; Ebe, H.; Hoshi, K.; Sato, J.; Sato, S.; Pu, Y.-J.; Ohisa, S.; Kido, J. Anion-exchange red perovskite quantum dots

with ammonium iodine salts for highly efficient light-emitting devices. *Nat. Photonics* **2018**, *12* (11), 681−687.
(26) Kim, Y.-H.; Kim, S.; Kakekhani, A.; Park, J.; Park, J.; Lee, Y.-H.; Xu, H.; Nagane, S.; Wexler, R. B.; Kim, D.-H.; et al. Comprehensive defect suppression in perovskite nanocrystals for high-efficiency light-emitting diodes. *Nat. Photonics* **2021**, *15*, 148−155.
(27) Kim, Y. H.; Cho, H.; Heo, J. H.; Kim, T. S.; Myoung, N.; Lee, C. L.; Im, S. H.; Lee, T. W. Multicolored organic/inorganic hybrid perovskite light-emitting diodes. *Adv. Mater.* **2015**, *27* (7), 1248−1254.
(28) Lee, H.; Kim, K.; Song, O. Properties of Double Electron Transport Layered Perovskite Solar Cells with Different ZrO_2 Layer Thickness. *Taehan Kumsok·Chaeryo Hakhoechi* **2020**, *58* (1), 59−66.
(29) Jeong, J.; Song, D.; Choe, J.; Chung, C.-H.; Hong, K.-H. Computational Design of Highly Efficient and Robust Hole Transport Layers in Perovskite Solar Cells. *Taehan Kumsok·Chaeryo Hakhoechi* **2019**, *57* (8), 535−542.
(30) Liang, J.; Wang, C.; Wang, Y.; Xu, Z.; Lu, Z.; Ma, Y.; Zhu, H.; Hu, Y.; Xiao, C.; Yi, X.; et al. All-Inorganic Perovskite Solar Cells. *J. Am. Chem. Soc.* **2016**, *138* (49), 15829−15832.
(31) Qiu, L.; Yang, H.; Dai, Z.; Sun, F.; Hao, J.; Guan, M.; Dang, P.; Yan, C.; Lin, J.; Li, G. Highly Efficient and Stable $CsPbBr_3$ Perovskite Quantum Dots by Encapsulation in Dual-Shell Hollow Silica Spheres for WLEDs. *Inorg. Chem. Front.* **2020**, *7* (10), 2060−2071.
(32) Sun, C.; Wang, X.; Xu, Y.; Lu, W.; Teng, X.; Fu, G.; Yu, W. Physical Origins of High Photoluminescence Quantum Yield in α-$CsPbI_3$ Nanocrystals and Their Stability. *Appl. Surf. Sci.* **2020**, *508* (1), 145188.
(33) Yao, H.; Zhao, J.; Li, Z.; Ci, Z.; Jin, Z. Research and progress of black metastable phase $CsPbI_3$ solar cells. *Mater. Chem. Front.* **2021**, *5* (3), 1221−1235.
(34) Dutta, A.; Pradhan, N. Phase-Stable Red-Emitting $CsPbI_3$ Nanocrystals: Successes and Challenges. *ACS Energy Lett.* **2019**, *4* (3), 709−719.
(35) Marronnier, A.; Roma, G.; Boyer-Richard, S.; Pedesseau, L.; Jancu, J.-M.; Bonnassieux, Y.; Katan, C.; Stoumpos, C. C.; Kanatzidis, M. G.; Even, J. Anharmonicity and Disorder in the Black Phases of Cesium Lead Iodide Used for Stable Inorganic Perovskite Solar Cells. *ACS Nano* **2018**, *12* (4), 3477−3486.
(36) Swarnkar, A.; Marshall, A. R.; Sanehira, E. M.; Chernomordik, B. D.; Moore, D. T.; Christians, J. A.; Chakrabarti, T.; Luther, J. M. Quantum Dot−Induced Phase Stabilization of α-$CsPbI_3$ Perovskite for High-Efficiency Photovoltaics. *Science* **2016**, *354* (6308), 92−95.
(37) Lee, D. E.; Kim, S. Y.; Jang, H. W. Lead-Free All-Inorganic Halide Perovskite Quantum Dots: Review and Outlook. *Han'guk Seramik Hakhoechi* **2020**, *57*, 455−479.
(38) Dong, Y.; Wang, Y.-K.; Yuan, F.; Johnston, A.; Liu, Y.; Ma, D.; Choi, M.-J.; Chen, B.; Chekini, M.; Baek, S.-W.; et al. Bipolar-shell resurfacing for blue LEDs based on strongly confined perovskite quantum dots. *Nat. Nanotechnol.* **2020**, *15* (8), 668−674.
(39) De Roo, J.; Ibáñez, M.; Geiregat, P.; Nedelcu, G.; Walravens, W.; Maes, J.; Martins, J. C.; Van Driessche, I.; Kovalenko, M. V.; Hens, Z. Highly dynamic ligand binding and light absorption coefficient of cesium lead bromide perovskite nanocrystals. *ACS Nano* **2016**, *10* (2), 2071−2081.
(40) He, K.; Shen, C.; Zhu, Y.; Chen, X.; Bi, Z.; Marimuthu, T.; Xu, G.; Xu, X. Stable Luminescent CsPbI3 Quantum Dots Passivated by (3-Aminopropyl) triethoxysilane. *Langmuir* **2020**, *36* (34), 10210−10217.
(41) Mir, W. J.; Swarnkar, A.; Nag, A. J. N. Postsynthesis Mn-Doping in $CsPbI_3$ Nanocrystals to Stabilize the Black Perovskite Phase. *Nanoscale* **2019**, *11* (10), 4278−4286.
(42) Van der Stam, W.; Geuchies, J. J.; Altantzis, T.; Van Den Bos, K. H.; Meeldijk, J. D.; Van Aert, S.; Bals, S.; Vanmaekelbergh, D.; de Mello Donega, C. Highly Emissive Divalent-Ion-Doped Colloidal $CsPb_{1-x}M_xBr_3$ Perovskite Nanocrystals through Cation Exchange. *J. Am. Chem. Soc.* **2017**, *139* (11), 4087−4097.
(43) Wang, H.; Sui, N.; Bai, X.; Zhang, Y.; Rice, Q.; Seo, F. J.; Zhang, Q.; Colvin, V. L.; Yu, W. W. Emission Recovery and Stability Enhancement of Inorganic Perovskite Quantum Dots. *J. Phys. Chem. Lett.* **2018**, *9* (15), 4166−4173.
(44) Mubiayi, K. P.; Moloto, N.; Moloto, M. J. Effect of Diphenylphosphinic Acid on Cesium Lead Iodide Perovskite Stability. *CrystEngComm* **2018**, *20* (35), 5275−5280.
(45) Liu, F.; Zhang, Y.; Ding, C.; Kobayashi, S.; Izuishi, T.; Nakazawa, N.; Toyoda, T.; Ohta, T.; Hayase, S.; Minemoto, T.; Yoshino, K.; Dai, S.; Shen, Q. Highly Luminescent Phase-Stable $CsPbI_3$ Perovskite Quantum Dots Achieving Near 100% Absolute Photoluminescence Quantum Yield. *ACS Nano* **2017**, *11* (10), 10373−10383.
(46) Xu, L.; Li, J.; Cai, B.; Song, J.; Zhang, F.; Fang, T.; Zeng, H. A bilateral interfacial passivation strategy promoting efficiency and stability of perovskite quantum dot light-emitting diodes. *Nat. Commun.* **2020**, *11* (1), 1−12.
(47) Hou, Y.; Zhou, Z. R.; Wen, T. Y.; Qiao, H. W.; Lin, Z. Q.; Ge, B.; Yang, H. G. Enhanced Moisture Stability of Metal Halide Perovskite Solar Cells Based on Sulfur−Oleylamine Surface Modification. *Nanoscale Horiz.* **2019**, *4* (1), 208−213.
(48) Shao, Y.; Xiao, Z.; Bi, C.; Yuan, Y.; Huang, J. Origin and elimination of photocurrent hysteresis by fullerene passivation in $CH_3NH_3PbI_3$ planar heterojunction solar cells. *Nat. Commun.* **2014**, *5* (1), 1−7.
(49) Koscher, B. A.; Swabeck, J. K.; Bronstein, N. D.; Alivisatos, A. P. Essentially Trap-Free $CsPbBr_3$ Colloidal Nanocrystals by Postsynthetic Thiocyanate Surface Treatment. *J. Am. Chem. Soc.* **2017**, *139* (19), 6566−6569.
(50) Motazedian, F.; Wu, Z.; Zhang, J.; Shariat, B. S.; Jiang, D.; Martyniuk, M.; Liu, Y.; Yang, H. Determining Intrinsic Stress and Strain State of Fibre-Textured Thin Films by X-ray Diffraction Measurements Using Combined Asymmetrical and Bragg-Brentano Configurations. *Mater. Des.* **2019**, *181* (5), 108063.
(51) Bodnarchuk, M. I.; Boehme, S. C.; ten Brinck, S.; Bernasconi, C.; Shynkarenko, Y.; Krieg, F.; Widmer, R.; Aeschlimann, B.; Gunther, D.; Kovalenko, M. V.; Infante, I. Rationalizing and controlling the surface structure and electronic passivation of cesium lead halide nanocrystals. *ACS Energy Lett.* **2019**, *4* (1), 63−74.
(52) Wang, H.; Zhang, X.; Sui, N.; Hu, Y.; Colvin, V. L.; Yu, W. W.; Zhang, Y. Photoluminescence Loss and Recovery of α-CsPbI3 Quantum Dots Originated from Chemical Equilibrium Shift of Oleylammonium. *ACS Appl. Mater. Interfaces* **2020**, *12* (10), 11769−11777.
(53) Kim, Y.-H.; Wolf, C.; Kim, Y.-T.; Cho, H.; Kwon, W.; Do, S.; Sadhanala, A.; Park, C. G.; Rhee, S.-W.; Im, S. H.; Friend, R. H.; Lee, T.-W. Highly efficient light-emitting diodes of colloidal metal−halide perovskite nanocrystals beyond quantum size. *ACS Nano* **2017**, *11* (7), 6586−6593.
(54) Eperon, G. E.; Paternò, G. M.; Sutton, R. J.; Zampetti, A.; Haghighirad, A. A.; Cacialli, F.; Snaith, H. J. Inorganic Caesium Lead Iodide Perovskite Solar Cells. *J. Mater. Chem. A* **2015**, *3* (39), 19688−19695.
(55) Huang, H.; Xue, Q.; Chen, B.; Xiong, Y.; Schneider, J.; Zhi, C.; Zhong, H.; Rogach, A. L. Top-Down Fabrication of Stable Methylammonium Lead Halide Perovskite Nanocrystals by Employing a Mixture of Ligands as Coordinating Solvents. *Angew. Chem.* **2017**, *129* (32), 9699−9704.
(56) Yang, S.; Chen, S.; Mosconi, E.; Fang, Y.; Xiao, X.; Wang, C.; Zhou, Y.; Yu, Z.; Zhao, J.; Gao, Y.; De Angelis, F.; Huang, J. Stabilizing halide perovskite surfaces for solar cell operation with wide-bandgap lead oxysalts. *Science* **2019**, *365* (6452), 473−478.
(57) Zhang, X.; Lu, M.; Zhang, Y.; Wu, H.; Shen, X.; Zhang, W.; Zheng, W.; Colvin, V. L.; Yu, W. W. PbS-Capped $CsPbI_3$ Nanocrystals for Efficient and Stable Light-Emitting Devices Using p−i−n Structures. *ACS Cent. Sci.* **2018**, *4* (10), 1352−1359.

https://doi.org/10.1021/acsphotonics.0c01952
ACS Photonics 2021, 8, 1979−1987